Video Article

Test Samples for Optimizing STORM Super-Resolution Microscopy

Daniel J. Metcalf[1], Rebecca Edwards[1], Neelam Kumarswami[1], Alex E. Knight[1]

[1]Analytical Science Division, National Physical Laboratory

Correspondence to: Daniel J. Metcalf at daniel.metcalf@nikon.co.uk

URL: http://www.jove.com/video/50579
DOI: doi:10.3791/50579

Keywords: Molecular Biology, Issue 79, Genetics, Bioengineering, Biomedical Engineering, Biophysics, Basic Protocols, HeLa Cells, Actin Cytoskeleton, Coated Vesicles, Receptor, Epidermal Growth Factor, Actins, Fluorescence, Endocytosis, Microscopy, STORM, super-resolution microscopy, nanoscopy, cell biology, fluorescence microscopy, test samples, resolution, actin filaments, fiducial markers, epidermal growth factor, cell, imaging

Date Published: 9/6/2013

Citation: Metcalf, D.J., Edwards, R., Kumarswami, N., Knight, A.E. Test Samples for Optimizing STORM Super-Resolution Microscopy. *J. Vis. Exp.* (79), e50579, doi:10.3791/50579 (2013).

Abstract

STORM is a recently developed super-resolution microscopy technique with up to 10 times better resolution than standard fluorescence microscopy techniques. However, as the image is acquired in a very different way than normal, by building up an image molecule-by-molecule, there are some significant challenges for users in trying to optimize their image acquisition. In order to aid this process and gain more insight into how STORM works we present the preparation of 3 test samples and the methodology of acquiring and processing STORM super-resolution images with typical resolutions of between 30-50 nm. By combining the test samples with the use of the freely available rainSTORM processing software it is possible to obtain a great deal of information about image quality and resolution. Using these metrics it is then possible to optimize the imaging procedure from the optics, to sample preparation, dye choice, buffer conditions, and image acquisition settings. We also show examples of some common problems that result in poor image quality, such as lateral drift, where the sample moves during image acquisition and density related problems resulting in the 'mislocalization' phenomenon.

Video Link

The video component of this article can be found at http://www.jove.com/video/50579/

Introduction

Recently a range of optical microscopy techniques have been developed, typically referred to as super-resolution microscopy or nanoscopy, which can bypass the diffraction limit and generate images with resolutions of 100 nm or better [1,2] . Since the announcement of super-resolution microscopy as being the Nature Methods method of the year in 2008, there has been a great deal of development of localization-based microscopes. For example, there are multi-color applications [3-6] , 3D implementations [7-12], and even live cell applications [5,13-17] . Moreover, as these systems are being commercialized and are now making their way out of optics laboratories into the hands of cell biologists there is likely to be a further increase in their use and application to biomedical questions.

One branch of this family is the localization-based methods which work by building up an image molecule-by-molecule. In order to do this, the majority of fluorescent molecules within the sample must be switched off so that only a few spatially-separated molecules are active at any one time. These molecules are then rapidly switched on and off and many images are taken so that a significant part of the population is imaged to reflect the underlying structure with sub-diffraction precision. A number of approaches have been published including GSDIM [18], PALM [19] , fPALM [20] , STORM [21] and RESOLFT [22]. Algorithms that measure the position of a single molecule detection can then be used to locate the actual position of the molecule with precisions better than 20 nm using Gaussian fitting[23], for example rapidSTORM [24,25] QuickPALM [26], palm3d [12] and rainSTORM[27]. When imaging cell or other biological samples, which have a high molecule density, it is therefore necessary to take many thousands of frames of this blinking, spatially separated, signal in order to image a significant proportion of the labeled molecules.

Stochastic optical reconstruction microscopy (STORM) and the highly related dSTORM and GSDIM methods are localization-based super-resolution methods, which have been demonstrated to work with commercially available organic dyes [21]. They have since been shown to be applicable to a number of different dyes [28-30], which makes the methodology particularly attractive because of the specificity and relative convenience of well-established immunolabeling approaches to perform fluorescence microscopy. Consequently, there is easy access to a range of dye-antibody and dye-biomolecule conjugates, which have the potential to be used in localization-based super-resolution imaging. Whilst the general principles of STORM and similar approaches are relatively simple, and at first sight the hardware and sample preparation seem relatively straightforward, there are a number of steps in the process which are critical to achieving high quality, artifact-free, super-resolution images.

As with all microscopy techniques the process can be thought of in 3 main steps: first, sample preparation, second, image acquisition and, third, image processing and/or image analysis and interpretation. The additional resolving power and method of generating super-resolution images using a localization-based approach introduces some new problems and considerations [31-33]. Starting with sample preparation, when performing immunolabeling, particularly indirect immunofluorescence where a primary and secondary antibody combination is used, it should be noted that the fluorescent dye may be up to 20 nm away from the molecule of interest. In the case of microtubules, this results in diameters of

35-50 nm compared with an expected microtubule diameter of 25 nm [28,30] . Also, the labeling density should meet the Nyquist criteria in order to generate a high quality image [14]. For example for an anticipated image resolution of 20 nm along a filamentous structure there should be a dye molecule at least every 10 nm [27]. Whilst many dyes have been published to work for localization-based approaches the overall performance of the dye is a mix of at least four important criteria, namely detected photons per switching event (the brightness of each blink - brighter is better), the equilibrium on-off duty cycle (the contrast ratio of dyes in the off versus on state - more off is generally better), the survival fraction (a low bleaching rate is better) and the number of switching cycles (the number of blinks per fluorophore - more is better for high resolution, although 1 blink per fluorophore can be an advantage for molecule counting purposes). The situation is further complicated by the fact that these properties for any given dye can vary in different buffer conditions and with laser power [28,29] . In addition, as well as these unique STORM considerations, image quality can be improved by optimizing sample preparation in the same way as more traditional fluorescence microscopy techniques for example by minimizing autofluorescence by modification of fixation conditions and the use of quenching reagents. Also, minimizing non-specifically bound fluorophores is important, which can be done by adjusting label concentrations, incubation times and blocking and washing steps.

The second step of image acquisition is also critical. The optimum settings on the microscope will depend on the dye, buffer conditions, labeling density, and sample type, *e.g.* monolayers on glass, cells or tissue samples. The main considerations are camera exposure time, frame number, illumination angle (TIRF, HILO, Epi) and laser power. The aim is to collect as many bright spatially separated blinks as quickly as possible. If the background is very high or the blinks are not very bright, in other words the signal-to-noise ratio is poor, the reconstruction algorithm will not be able to localize the positions as accurately. As well as maximizing the localization precision, *i.e.* the accuracy with each molecule position can be measured, image quality also depends on a high number of localizations. If an insufficient number of the molecules of interest are imaged, either due to poor labeling efficiency, excessive photobleaching or an inadequate frame number, then the resulting super-resolution image will be punctate and discontinuous as Nyquist criteria will not have been met [14,27].

And finally, the third step, image processing, is particularly important compared with standard fluorescence microscopy techniques. There is a range of freely and commercially available algorithms, which is both an advantage, in terms of choice, and a disadvantage, in that it can be confusing to know which is most appropriate to use. If for example the raw data has well-spaced spatially distinct blinks then a single-molecule fitting algorithm can be highly accurate and efficient, for example by the sparse fitting algorithms available in rainSTORM [27], rapidSTORM [24,25] , palm3d [12] and QuickPALM [26]software. If the raw data contains a lot of overlapping signals then algorithms which may be more appropriate include DAOSTORM [34], 3B [35] and deconSTORM [36]. Moreover, these algorithms contain thresholds for various criteria such as signal counts, or photons per blink, as well as various different image display options such as visualizing with smoothed Gaussian functions or as histograms with pixel grids, where the super-resolution pixel size can be selected by the user. All of these options change the appearance of the final image and have implications for image interpretation and analysis.

Therefore, we present 3 test samples which will provide the new user with a starting point for dye-based localization-based super-resolution experiments, which for the sake of clarity we will refer to as STORM, and more experienced users the opportunity to further optimize their experiments. First, it is possible to coat the surface of glass with a fluorescent layer of dextran-dye conjugate. This provides a quick and simple way to establish that the microscope, dye and buffer are working to generate blinking fluorescent signal. The method can then be extended by comparing mean localization precision and number metrics generated by rainSTORM to optimize buffer conditions, image acquisition settings and test different dyes. Second, we present a simple protocol for preparing actin filaments on glass which can be readily labeled using phalloidin-dye conjugates. These provide ideal structures to take measurements of resolution [27] and typically the full width half maximum (FWHM) of a filament is given as an empirical estimate of resolution [37]. It should be noted that resolution varies between samples and between images within the same sample because resolution in localization-based super-resolution microscopy is a function of fluorophore brightness, background noise and localization density [27] and these are not necessarily constant throughout the specimen. Actin filaments are used to demonstrate potential artifacts such as mislocalizations and drift and how they can be identified with software features within rainSTORM. Moreover, we describe the use of fluorescent fiducial markers to both measure and correct drift. And third, the staining of cells with epidermal growth factor (EGF)-dye conjugates is described. EGF provides a useful indicator of super-resolution image performance, because a proportion of the receptor at the cell surface undergoes endocytosis via vesicles, which are sub-diffraction sized structures of approximately 50-150 nm in diameter [27,38,39] .

Protocol

Note: Throughout this protocol, tips and suggestions are found following certain steps. The notation "*1" indicates that note 1 is relevant to this specific step, and so on.

1. Fluorescent Dextran Coating of Glass

1. Add 200 µl of 0.01% poly-L-lysine solution to each well of an 8-chamber coverglass and incubate for 10 min. Remove with a pipette to ensure that no is liquid remaining.
2. Reconstitute dextran-Alexa 647[*1] according to manufacturer's instructions to create a 2 mg/ml stock solution. From this, dilute 0.25 µl into 25 µl of de-ionized water to create a 20 µg/ml solution.
3. To create a high density coating of dextran-Alexa 647 solution dilute 20 µl of the 20 µg/ml solution into a total of 200 µl of de-ionized water. For a medium density solution dilute 2 µl in 200 µl of de-ionized water (1:10,000 dilution from the original stock solution). For a low density solution dilute 0.2 µl in 200 µl of de-ionized water (1:100,000 dilution from the original stock solution).
4. Add 200 µl of the diluted dextran-Alexa 647 solutions to each well and incubate for 10 min. Longer incubation times can be used which may result in a denser dextran coating. Remove and wash with H_2O three times[*2]

Note 1: Other dextran-dye conjugates can be used. Unconjugated dextran can also be conjugated to dyes if desired combinations are not commercially available.

Note 2: The same dextran chambers can be reimaged over a period of weeks although the uniformity of the fluorescence may decrease. Storage at 4 °C in the absence of any buffer is recommended.

2. Fluorescent Actin Filaments on Glass

1. Add 200 µl of 0.01% poly-L-lysine solution to each well of the chamber and incubate for 10 min[*3]. Remove with a pipette to ensure that no liquid is remaining.
2. Add 90 µl of general actin buffer (reconstituted according to manufacturer's instructions) to each chamber. Add 10 µl of 10 µM preformed actin filament solution and 1 µl phalloidin-Alexa 647 (0.2 units, when dissolved in 1.5 ml of methanol as per manufacturer's instructions) and gently pipette up and down to mix. Incubate for 30 min[*4].

Note 3: Increasing the volume of the filament solution within the chamber results in fewer filaments binding to the poly-L-lysine coated glass.

Note 4: Incubation times of up to 48 hr at 4 °C have been tested with good results. Actin filament image quality deteriorates once a chamber has been exposed to switching buffer so it is not recommended to use the same sample for more than one day.

3. Microsphere Fluorescent Beads as Fiducial Markers

1. Dilute 1 µl of TetraSpeck beads into 200 µl PBS and mix.
2. Add the diluted beads into an imaging chamber and wait for 15 min[*5]. Remove the solution and wash 3 times with PBS prior to imaging.

Note 5 - the dilution and incubation time can be adjusted to obtain different densities of beads. This protocol typically results in between 3 - 10 beads per 20.5 µm x 20.5 µm field-of-view.

4. Epidermal Growth Factor Cell Staining

1. Culture HeLa cells in imaging chambers to approximately 80% confluency in Dulbecco's Modified Eagle Medium (DMEM) supplemented with 10% fetal bovine serum (FBS) and 1% penicillin-streptomycin solution.
2. Remove the culture medium and wash with PBS. Then add 500 µl of 4% formaldehyde solution (4 ml 10% formaldehyde solution, 1 ml 10X PBS, 5 ml water) for 10 min. Remove the formaldehyde and wash 3 times with PBS. Do not allow the cells to remain dry and always use PBS buffered solutions to avoid hypotonic stress.

CAUTION - formaldehyde is extremely toxic. Ensure that appropriate gloves, eye protection and lab coats are worn. Check local guidelines for disposal of formaldehyde.

3. Reconstitute EGF-Alexa 647 according to manufacturer's instructions to create a 50 µg/ml stock solution. Add 2 µl of this stock solution to 200 µl of 0.1% BSA solution (in PBS). Remove the PBS from the cells, add the EGF solution and incubate for 30 min.
4. Remove solution and wash 3 times with PBS before adding a blocking solution of 0.1% BSA (in PBS) for 15 min. Remove this and wash a further 3 times with PBS prior to imaging.

5. Switching Buffer Preparation

1. Make an enzyme stock solution (A) with 10 µl of catalase (20 µg/ml), 20 µl of 1 M Tris (2-carboxyelthyl) phosphine hydrochloride (4 mM), 2.5 ml glycerin (50%), 125 µl of 1 M KCl (25 mM), 100 µl of 1 M pH 7.5 Tris-HCl (20 mM), 5 mg of glucose oxidase (1 mg/ml) and top up to 5 ml volume with diH20. This is sufficient to make 100 x 50 µl aliquots, which can be stored at -20 °C and used for up to 1 year.
2.) Make a glucose stock solution (B) with 4 g glucose (100 mg/ml), 4 ml glycerin (10%) and 36 ml diH20. This is sufficient to make 100 x 400 µl aliquots, which can be stored at - 20 °C and used for up to 1 year.
3. Make a reducing agent stock solution (C) with 113.6 mg of MEA-HCl (1M) and 1 ml of di$H_2$0. Use fresh or make 10 x 100 µl aliquots, which can be stored at -20 °C and used for up to 1 month (do not refreeze aliquots).
4. Just prior to imaging, mix the enzyme (A), glucose (B) and reducing agent (C) stock solutions together in the ratio 50 µl, 400 µl, 100 µl and make up to 1 ml with PBS[*6]. This buffer will now scavenge oxygen and have a reducing environment (100 mM MEA-HCl)[*7]. The final pH should be in the range 6.0 - 8.5 (adjustment is not normally necessary)[*8].

Note 6 - this buffer is suitable for use with carbocyanine-based dyes such as Cy5 and Alexa 647.

Note 7 - the final enzyme concentrations are 50 µg/ml (5 unit/ml) of glucose oxidase and 1 µg/ml (40-60 units/ml) of catalase. The enzymatic activity (units) is given by suppliers and can vary. The calculations for catalase assume that 1 µg/ml final concentration after step 5.4 will contain 50 units of enzyme. Various buffer compositions including similar oxygen scavenging components can be found [21,30,40]. For a summary of buffer and dye combinations see references [28,29]. Glycerin and TCEP are required for long-term storage at -20 °C.

Note 8 - if imaging actin filaments add 2 mM $MgCl_2$ and 0.2 mM ATP to help stabilize the filaments.

6. Microscope Acquisition of STORM Data (using Alexa 647 dye)

1. Switch on the STORM/PALM microscope, preferably at least 3 hr before imaging to allow a thermal equilibrium to be reached. Imaging before this has an increased chance of drift.
2. Insert the imaging chamber into the microscope stage sample holder. Ensure that the sample is firmly in the holder and is flat.

3. Remove the PBS from the imaging chamber and then fill to the top with the switching buffer. Carefully place a coverslip over the top of the chamber, making sure that there are no bubbles at all and that the entire chamber is covered. Top up with additional buffer or PBS if any bubbles are seen otherwise buffer performance can decline.

CAUTION - to minimize the chances of lateral and axial drift of the sample in relation to the objective lens it is recommended that the sample and the buffer are left to equilibrate to room temperature for at least 15 min prior to imaging.

4. Locate a fluorescent structure of interest to be imaged. Select the desired angle of illumination, in this case, a TIRF or highly inclined angle is recommended as this improves the signal-to-noise ratio by minimizing out-of-focus light, which is particularly of benefit for cell samples. Take a reference diffraction-limited image of the structure prior to STORM imaging.
5. Increase the excitation laser (with an appropriate excitation wavelength of approximately 640 nm) to a high power, corresponding to approximately 2 kW/cm^2 whilst imaging with camera settings of 10 msec exposure and a cycle time of approximately 50 Hz (frames per second). Once the fluorophores have transitioned into a sparse blinking pattern (probably within 10 sec for most samples) collect 10,000 frames[*9].

Note 9 - 10,000 frames is suitable for the samples described here but it may be necessary to increase the frame number to 50,000 or more for other samples.

7. Reconstructing Super-Resolution Images from Raw Data (using rainSTORM)

1. Open the rainSTORM.m file from within MATLAB and run (**Figure 1A**).
2. In the rainSTORM window (**Figure 1B**) select the image file to be analyzed using the browse button. This should be a .tif file (ImageJ can be used to convert other file types into a tif format). Alter the pixel width to match the raw data of the microscope system used to acquire the data[*10]. Leave the other values to default.

Note 10 - A typical EMCCD camera has a pixel size of 16 µm so on a system with a 100X objective lens the pixel size on the image will be 160 nm. On commercial systems the pixel size is usually displayed within the software. Pixel sizes vary between 100 nm and 160 nm for most localization microscopes.

3. Press the 'Process Images' button and wait until a preliminary image appears. The duration of the processing will depend on the file size, computer specification and the number of candidate blinks within the raw data[*11].

Note 11 - 10,000 frame sequences of actin and EGF data took 23 sec and 25 sec to process respectively using a PC with an Intel Xeon E5420 CPU. Using the same computer without a parallel processing toolbox in MATLAB, or with a computer without multiple core processing, times were 66 sec and 81 sec respectively.

4. To generate an updated super-resolution image press the 'Open Reviewer' button and a second window will appear (**Figure 1C**). Press the 'Adjust Contrast' button in order to change the image display as desired (**Figure 1D**). In some cases, where the image is very dark the maximum value should be decreased.
5. Use the reviewer window (**Figure 1C**) to generate useful image quality metrics and refine the super-resolution image further. Set the first three quality control parameters to values of 4,000, 0.1 and 0.8-2.0 respectively[*12]. Update the counts per photon value, which should either be based on a photon calibration measurement or using photon-curve calibration curve values specified by the camera manufacturer for a particular EM gain setting. This is critical for obtaining accurate precision and resolution measurements[*13].

Note 12 - Signal Counts rejects blinks based on brightness criteria. The higher the value the brighter the blink must be to become accepted as a localization in the final image. This may need to be altered depending on the photon output of the dye and exposure time and sensitivity of the camera. Tolerance rejects blinks if there is significant square error between the signal and the fitted Gaussian i.e. double peaks. PSF Sigma Range rejects blinks if the fitted width of the PSF lies out of this range, i.e. a narrower range can be used to reject out-of-focus signals and large aggregated blobs of constant fluorescence. Using a wider range may result in mislocalization artifacts appearing in the final image. In practice, it is recommended to perform initial quality control using the localization precision cutoff parameter.

Note 13 - for more on resolution metrics see references [23,27]. In brief by knowing the number of photons produced by each blink it is possible to calculate the localization precision of each localization and consequently derive overall mean precision estimates for the entire image. Using an Andor iXON DU-897E with a gain setting of 200 the Counts per Photon value is 9.04.

6. Alter the localization precision cutoff (**Figure 1C**) to tradeoff between optimizing mean localization precision against localization number in the final image. Values of 30-50 nm are recommended depending on the quality of the data and the sample. Both the histograms and the info.txt files can be used to inform this decision (**Figures 1F and 1G**).
7. The reconstruction scale factor (**Figure 1C**) default is 5, which will generate super-resolution pixels of 32 nm assuming that the pixel width in the original images is 160 nm. If the raw images have a pixel size of 100 nm this will produce super-resolution images with pixels of 20 nm. Increase the scale factor to produce smaller super-resolution pixels in the final image[*14].

*Note 14- Resolution of localization microscopy depends on the smoothing required for visualization (ie. the pixel size of a simple histogram reconstruction) as well as the localization precision. In practice, the reconstruction pixel size should generally be smaller than the localization precision (see the Mean Precision Estimate metric in the info text file - steps 6.11 & 6.12). In this case the loss of resolution due to reconstruction pixel size will be small [23,27]. For example the mean precision estimates in the row and column direction of **Figure 4E** are 16.1 nm and 16.2 nm. A pixel size of 16 nm has been used to visualize this data (reconstruction scale factor of 10 with an original pixel width of 160 nm).*

8. Modify the limit frame range (**Figure 1C**) to restrict the reconstruction to subsets of the raw data, for example [2001-inf] would exclude the initial 2,000 frames of raw data.
9. Press the 'Run Reviewer' button (**Figure 1C**) to generate an updated super-resolution image (**Figure 1E**).

10. Press the 'View Histograms' button (**Figure 1C**), in order to display image quality metrics (**Figure 1F**)[*15].

*Note 15 - The graph in the top right depicting the number of accepted localizations against camera frame number and the Thompson Localization Precisions histogram in the bottom right (**Figure 1F**) can be used to inform the localization precision cutoff review option. For example, using a 50 nm cutoff would exclude all the localizations with worse precision from being included in the final super-resolution image.*

11. Press the 'Save Image' button in the reviewer (**Figure 1C**) in order to save all of this data[*16].

*Note 16 - Between 3 and 5 files can be saved depending on the options selected (sum image, STORMdataImage, STORMprocessed, info & hists), see **Figure 1G**. The STORM processed image is displayed with modified contrast and color maps. The STORMdataImage is a grayscale image, in which the gray level of each pixel equals the number of localizations which were identified within it.*

12. After examining the data (*e.g.* Info.txt file and histograms) return to step 7.6 and repeat the subsequent steps with different reviewer parameters if desired. Pressing 'Save Image' in step 7.11 will overwrite the previously saved data.

8. Box Tracking and Drift Correction (using rainSTORM)

1. Follow steps 7.1 - 7.9 to generate an image in the normal way.
2. Press the 'Box Tracking' button in the reviewer (**Figure 1C**) and click and drag a box over the fiducial marker or structure of interest on the reviewed image.
3. Wait until a new image appears, which will display the 'Boxed Positions' (see **Figures 6B, 6C and 6F** for examples). Save this image if desired.
4. If the object of interest is a fiducial marker then drift correction can be performed by clicking the 'Set Anchor' button followed by the 'Subtract Drift' button. Finally click 'Run Reviewer' again to generate a new STORM image, which will now have all localizations corrected according to the fiducial marker positions. The bead positions are deleted from the final reviewed image.
5. If there are other fiducial markers within the final drift corrected image, these can be removed by pressing 'Box Tracking', 'Delete Boxed' and then 'Run Reviewer' as many times as desired.

Representative Results

Dextran

A successful coating of dextran should produce a fluorescent monolayer. At the high concentration this should appear relatively uniform. At lower concentrations it will appear sparser (**Figure 2A**). Many STORM/PALM microscopes have the ability to change the angle of illumination from epifluorescence to TIRF. When using a full frame camera view, for example at 512 x 512 pixels on a typical EMCCD camera, an even illumination should be observed. If there are any stripes or out-of-focus regions this can indicate that the sample should be reinserted into the sample holder with fresh oil on the objective lens. Alternatively it may indicate a problem with the microscope.

When acquiring super-resolution raw data the imaging laser should be increased in power to approximately 2 kW/cm^2. There will be an initial burst of fluorescence followed by blinking as the fluorophores are driven into temporary dark states. At high dextran densities the blinks are likely to overlap, particularly near the beginning of the image acquisition (**Video 1**). At medium and low densities these blinks should be sparse, *i.e.* spatially separated, and in focus with no obvious background (see frames 2,000, 5,000 and 8,000, **Figure 2A**, **Videos 2 and 3**). During this image acquisition phase, at constant laser illumination, the number of blinks will decrease with time (compare frame 2,000 with frame 8,000 in the high density sample, **Figure 2A**). The main difference between the various super-resolution images of the different dextran concentrations (high, medium and low) is the decreasing number of localizations (**Figures 2A and 2B**). In other words, the concentration of the fluorescent molecules, number of blinks in the raw data and the number of localizations have a proportional relationship. This relationship, however, is not a simple linear one as at very high molecule densities the software is unable to successfully localize molecules (compare the red and blue lines, **Figure 2C**). The reason for this is that at the high concentration it is not possible for the processing software to fit the positions using the Gaussian fitting algorithm where the blinks are non-sparse. As the blinks decrease through the acquisition phase due to photobleaching the software can fit more and more of the blinks as they become sparse (**Figures 2A and 2C**). Moreover, individual dye molecules may blink, and therefore be localized more than once [28,41,42].

A common problem when imaging any of these samples, but particularly the high density dextran one, can be the presence of bright but unfocused fluorescent haze that appears to be rapidly diffusing during the STORM image acquisition phase. This is distinct from the high contrast fluorophores on the surface of the glass, which can be seen blinking (**Figure 3A**, **Video 5**). These detached fluorescent molecules can be prevented or removed by increasing the number of wash steps with PBS prior to adding the switching buffer or by adding fresh switching buffer to the chamber (**Figure 3B**, **Video 6**). Processing and comparing the data from each image sequence results in very different super-resolution images which have a decrease in both the number of localizations and the precision with which they can be fitted of the software to localize the blinks (**Figures 3C, 3D, 3E and 3F**).

Actin Filaments

Preformed actin filaments can be seen stuck to the surface of the glass by diffraction-limited imaging (**Figure 4A-4C**). If the number of filaments appears very low, then a longer incubation time can be used or a decrease in the volume of the actin filament solution also helps. Selecting single relatively bright filaments (**Figure 4D**) rather than tangled areas results in better quality images. During the acquisition phase, bright in-focus blinks should be seen along the length of the filament (**Video 7**). Sparse blinking should be seen during the acquisition phase and then subsequently in the processed data there should be a thin continuous filament (**Figure 4E**) and the localizations per frame should a gradual decline (**Figure 4F**), unlike in **Figure 3E**.

If blinking is non-sparse, or if the software not being able to localize the molecules, a more subtle artifact, called a mislocalization [32], can result. This arises when the software averages the position of two overlapping molecules and the localization is position mid-way between them. An indication that there have not been a significant number of overlapping blinks, and consequently mislocalizations, is that the mean precision estimates should be the same in the row and column directions, *i.e.* horizontally and vertically; where there are mislocalizations these would have occurred along the length of the filament, produced a larger than normal blink (*i.e.* spread over more pixels), which would consequently have been localized with less accuracy in one of the directions. This is most easily seen where there is a single actin filament in the imaging area and it is lying horizontally or vertically. In this case, the STORM microscope, achieved a mean precision of 16 nm in both directions. This results in a precision limit, a measure of effective image resolution of approximately 34 nm. These metrics are provided by rainSTORM [27], however, as we have a filamentous structure of uniform diameter, 7 nm with the very small phalloidin-Alexa 647 label we can take a measure of FWHM to estimate the resolution of the image. By drawing a straight line through the filament of the super-resolution image in ImageJ (**Figure 4G**), using the plot profile feature (**Figure 4H**) and subsequently performing a Gaussian fit (**Figure 4I**) the FWHM is calculated as 43.2 nm. When attempting this measurement we recommend that the pixel size should match or be slightly smaller than the mean precision estimate for the image (see info.txt file **Figure 1G**). In this case, 16 nm pixels were used to reconstruct an image.

Two related problems can occur with STORM, where the blinking fluorophores become non-sparse, *i.e.* individual molecules within approximately 250 nm blink at the same time and therefore the signals overlap. The first is that depending on the algorithm and the quality control criteria it uses, the blinks may not be localized at all. This results in super-resolution images with few or no localizations. The second problem of mislocalizations occurs when the two blinks occurred sufficiently close to each other to appear as a single blink. In this case the position in the final image represents an average of the two. For more detail on this see reference [32]. In both cases this can occur with very high density samples, insufficient laser power or with switching buffer problems. This problem is apparent where a number of actin filaments are branching and/or crossing each other (**Figures 5A-D**, **Video 9**). By processing subsets of frames, and comparing the first and last 5,000 frames we can see a different resulting image. In the super-resolution image using the first 5,000 frames (**Figure 5C**) we can see that there are many localizations in the middle of the image, however when using the last 5,000 frames, very few of these are apparent and we are left with just the filaments, albeit somewhat discontinuous owing the low number of localizations in the image (**Figure 5D**). If a too high blinking density is suspected comparison of the images with the localization per frame data can strongly suggest that this problem is occurring; during the first set of frames there is an average number of localizations per frame of over 10 compared with the last set of frames where it is approximately 4 (**Figure 5E**). In order to minimize the likelihood of mislocalizations occurring it is ideal to have as few localizations per frame as possible, although if there are a large number of molecules to be imaged, *i.e.* for a high density sample, this requires that a large number of acquisition frames be taken leading to another problem in STORM microscopy which is drift.

Lateral Drift - Actin Filaments and Fiducial Markers

Drift occurs when the sample moves in relation to the objective lens through the data acquisition phase. This is difficult or impossible to see during the image acquisition phase, particularly if it is lateral rather than axial, or unless it is being specifically measured, as it is typically less than 50 nm over the course of several minutes for relatively stable microscope systems. However, in reconstructed images of known structures such as actin filaments with well-defined structure, it can be detected in the super-resolution images. The first sign that lateral drift may have occurred is that the structure is larger than expected (**Figure 6A**, **Video 8**) for example with a relatively large FWHM compared with the precision limit data from rainSTORM, in this case 90 nm compared with 67 nm. However, a better way to detect drift is by comparing the localizations as a function of time, *i.e.* seeing if the localizations in the later frames are displaced compared with those in early frames. This can be clearly seen in the case of actin filaments, which are very small and of uniform structure, when displayed with a color code using the box tracking feature in rainSTORM (**Figures 6B and 6C**).

Drift is a well-recognized problem and there are a number of strategies that can be used to minimize it [19] or correct it post-acquisition either using fiducial markers [21,43] or cross-correlations [44] . In order to measure drift and correct for it, fluorescent beads of 100 nm diameter can be used as fiducial markers (**Figure 6D**). Because they are small and bright their position can be accurately measure using Gaussian fitting algorithms, such as rainSTORM. In an example where there is relatively severe drift of approximately 100 nm over the course of 3 min 10 sec, during the acquisition phase (**Figure 6E**), the same box tracking feature can be used to color code and confirm that drift occurred (**Figure 6F**). As all four beads in this example show near-identical drift it is possible to select one of them, in this case bead 2, to use as reference and subtract the drift from the other beads (**Figure 6G**). By adding fiducial markers to a biological sample of interest it then becomes possible to measure and correct any drift where the underlying structure is unknown or far more variable than an actin filament or a fluorescent bead.

Epidermal Growth Factor

Finally, EGF-stained HeLa cells can be used to give a realistic example of image resolution in cells (**Figure 7A**, **Video 10**). These cells are relatively straightforward to image as they should have the majority of the EGF-fluorescence in the plane-of-focus on the cell surface in close proximity to the coverglass. The less bright region the in center corresponds to the position of the nucleus. TIRF illumination can enhance the image quality by eliminating out-of-focus fluorescence coming from parts of the cell membrane not in close proximity to the glass (approximately 150 nm penetration into cells). Zoomed in regions of interest in the diffraction-limited image are typically indistinct (**Figures 7B and 7C**), however in the super-resolution images there should be a mixture of clusters and occasional isolated single pixels (**Figures 7D-7F**). These will represent either isolated EGF receptors at the cell surface or possible a small amount of non-specific binding. The clusters will be approximately 100 nm in diameter and are likely to correspond to forming pits and vesicles, the pathway via which EGF is predominantly down-regulated and endocytosed. Typical mean precision estimates are around 20 nm for this type of sample with a precision limit of approximately 45 nm. It should be noted that this precision limit measure of effective resolution does not take into account label size, or any drift, which can be measured with fiducial markers, but is still noticeable by "comet tails" on the clusters or using the box tracking feature as outlined in **Figure 6** and described in protocol section 8.

Component	Final Concentration
Catalase	1 µg/ml (50 units)
Glucose	40 mg/ml

Glucose oxidase	50 µg/ml
Glycerin	12.50%
KCl	1.25 mM
MEA-HCl	100 mM
TCEP	200 µM
Tris	1 mM

Table 3. Switching buffer

Typical Acquisition Settings	**Value**
Pixel size (nm)	160
Exposure time (msec)	10
Gain	200
Frame size (pixels)	128 x 128
Cycle time (fps)	52.5
Frame number	10,000
640 nm laser power density (kW/cm^2)	2

Table 4. Acquisition settings

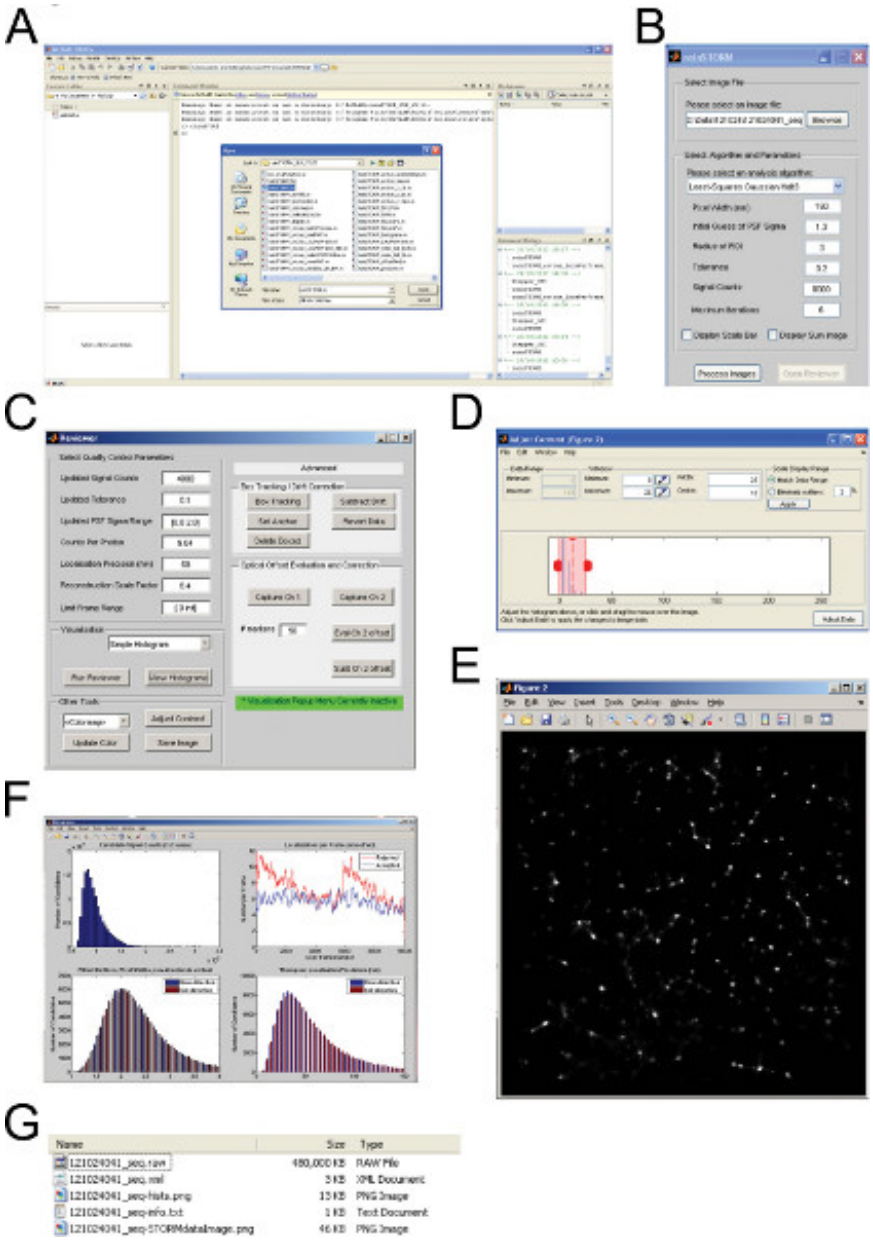

Figure 1. STORM Image Reconstruction Using rainstorm. (A) Opening rainSTORM from within MATLAB. (B) rainSTORM graphical user interface (GUI). (C) rainSTORM Reviewer GUI. (D) Adjust contrast window. (E) STORM image after review and contrast adjustment. (F) Histograms of image quality metrics. (G) Files generated after pressing save image button in reviewer GUI. Click here to view larger figure.

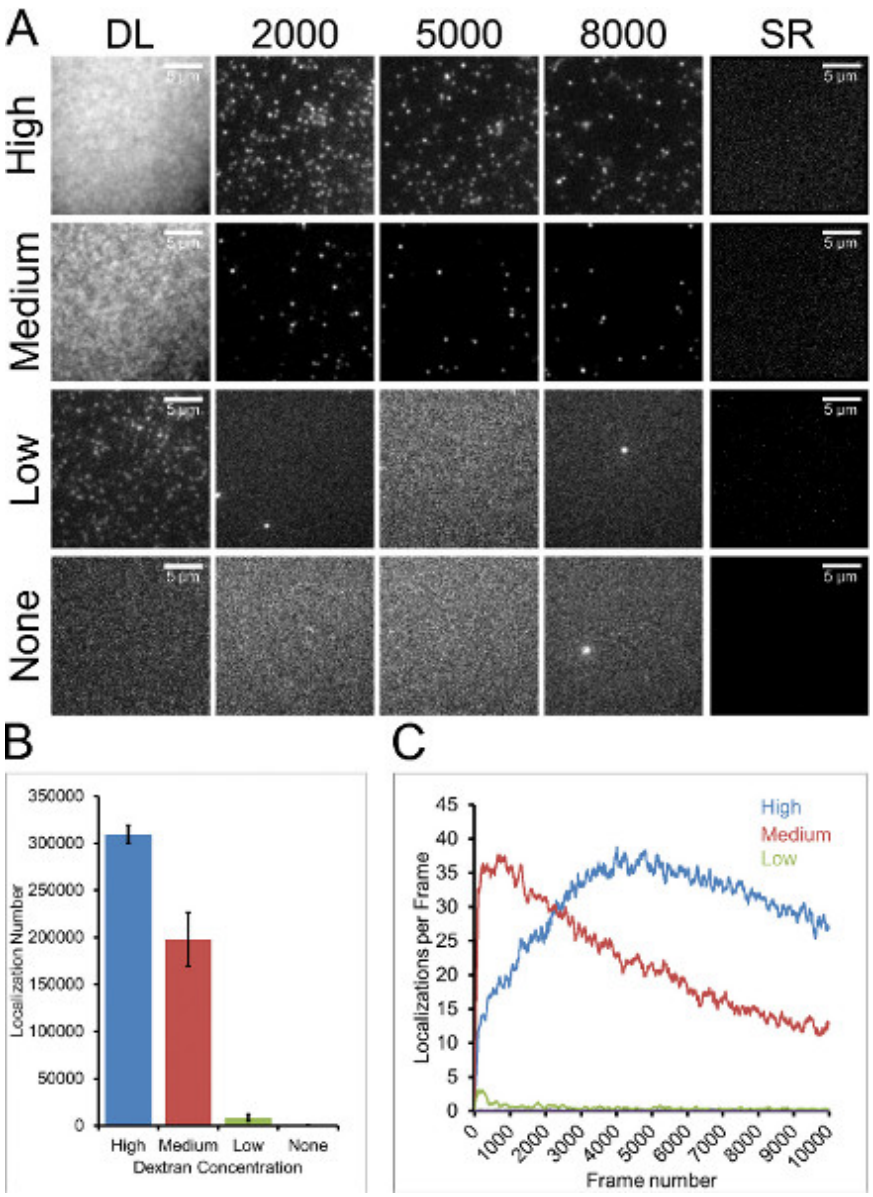

Figure 2. (A) Diffraction limited (DL) images show different concentrations of dextran prior to STORM imaging. Super-resolution (SR) image reconstructions have a pixel size of 25 nm. 10,000 images were collected with a 128 x 128 pixel frame size and individual frames are shown from that sequence (2,000, 5,000, 8,000). Acquired with a 10 msec exposure time at 52.5 frames per second. Images have a pixel size of 160 nm. For clarity of viewing a 0.1% pixel saturation contrast enhancement was applied using ImageJ. The mean precision estimates are 28 nm (high), 24 nm (medium) and 16 nm (low) for the different dextran images. The localization densities are 724 per μm^2 (high), 526 per μm^2 (medium) and 13 per um^2 (low). (B) Graph showing an average of three 10,000 frame sequences of each concentration of dextran. Error bars show standard deviation.(C) Graph plotting the number of accepted localizations per frame using a rolling 100 frame average. Click here to view larger figure.

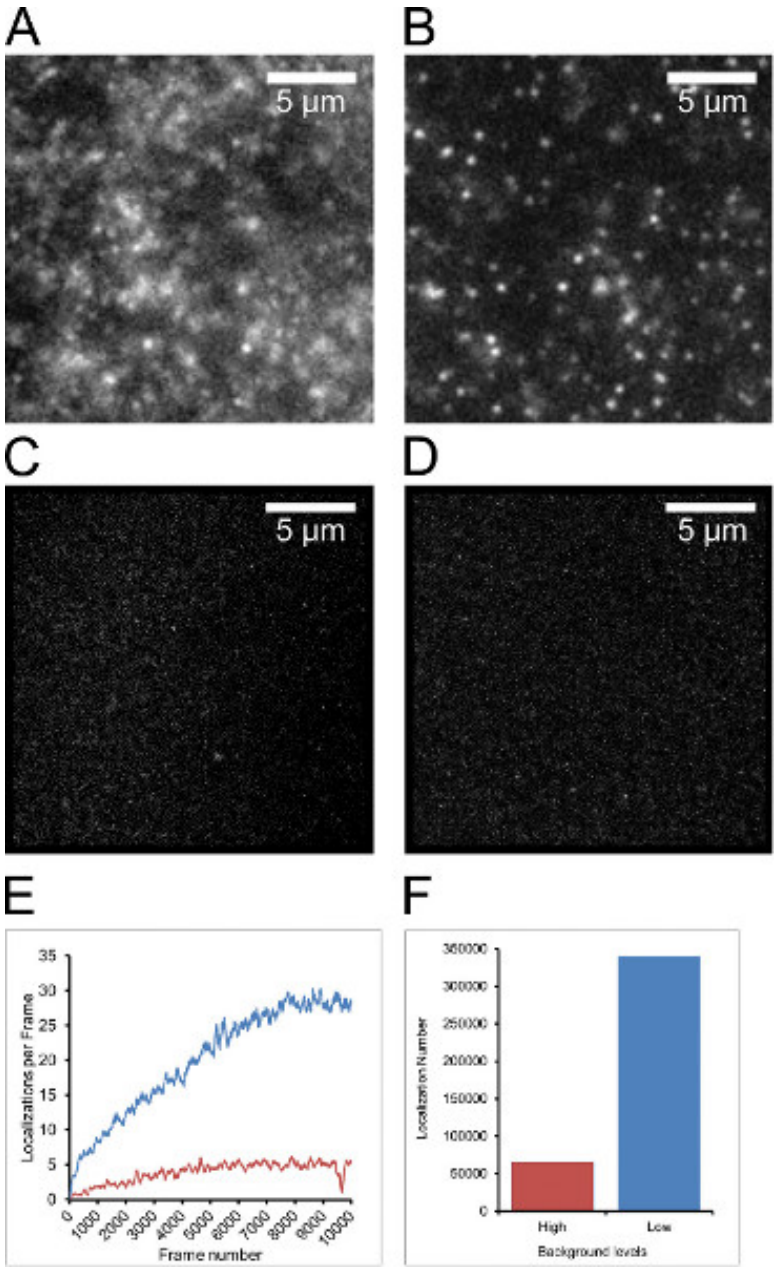

Figure 3. Poor Quality Dextran Data. (A) Diffraction limited frame from a 15,000 frame STORM sequence. Note the diffuse fluorescent haze across the image. This is caused by fluorophores diffusing through the medium. 128 x 128 pixel frame size, a 10 msec exposure time and acquired at 52.5 frames per second. (B) The same as (A) after the buffer had been changed. Note the improved contrast as unbound fluorophores have been washed away. (C) A super-resolution image reconstruction corresponding to the data collected in (A). Identical image size but with pixels of 25 nm. The mean precision estimate is 35 nm. (D) A super-resolution image reconstruction corresponding to the data collected in (B). Identical image size but with pixels of 25 nm. The mean precision estimate is 30 nm. (E) Graph plotting the number of accepted localizations per frame, using a rolling 100 frame average. The red line corresponds to STORM sequence (A & C) where there is a high background. The blue line shows data corresponding to (B & D), where the background is low. (F) Graph showing the accepted localization number for the images corresponding to high (C) and low (D) background data. Click here to view larger figure.

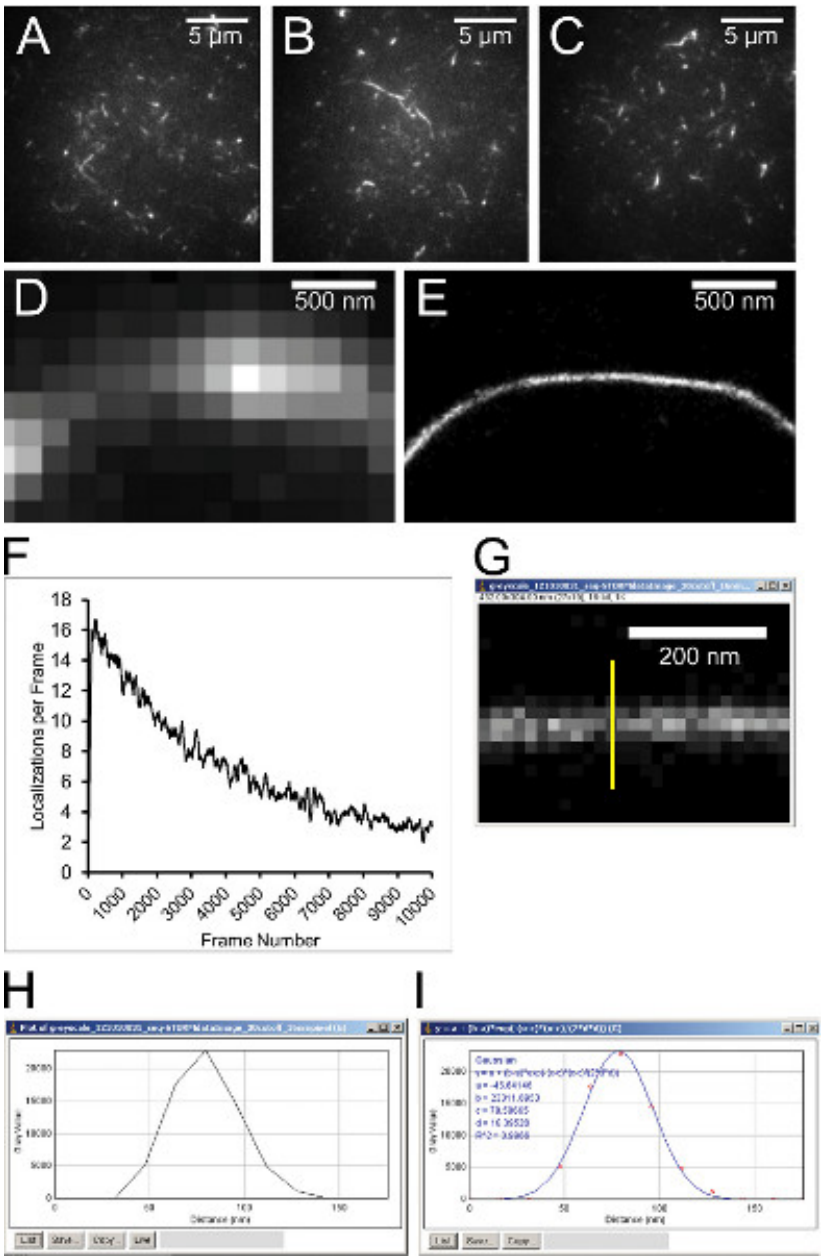

Figure 4. Typical Actin Data. (A-C) Diffraction-limited images of actin filaments prior to addition of switching buffer and STORM imaging. Variable lengths of filaments can be seen. Very bright filaments are often several filaments tangled together. Pixel size is 160 nm. (D) A diffraction-limited image of a single actin filament. (E) STORM image (0.1% contrast enhancement applied in ImageJ). From a 10,000 frame sequence with a 128 x 128 pixel frame size, a 10 msec exposure time and acquired at 52.5 frames per second. The pixel size is 16 nm. The mean precision estimate is 16 nm. (F) Graph plotting the number of accepted localizations per frame, using a rolling 100 frame average. (G) A zoomed in region of the actin filament from (E) prior to contrast enhancement with a yellow line profile drawn across. (H) A plot profile view from the yellow line drawn across the actin filament. Generated in ImageJ. (I) A Gaussian fit of the plot profile using the curve fitting tool in ImageJ. The standard deviation, d, was multiplied by 2.35 to get a FWHM measurement of 43.2 nm. Click here to view larger figure.

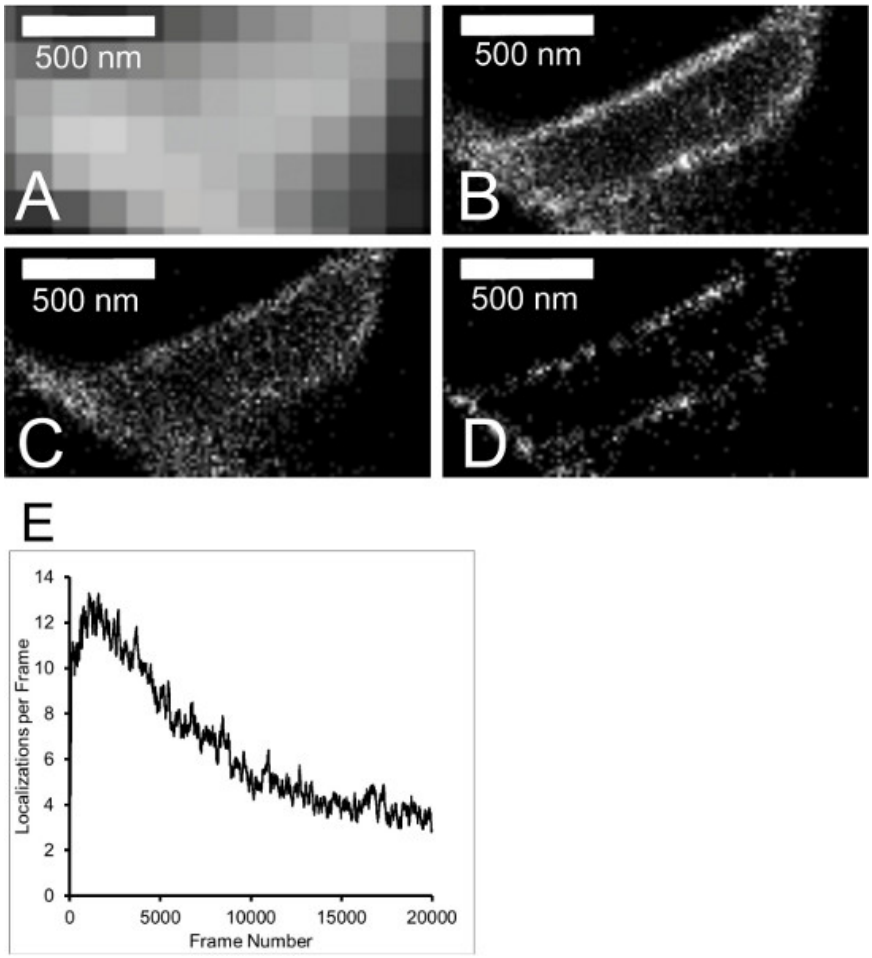

Figure 5. Mislocalized Actin Filaments. (A) Diffraction-limited actin filament. 160 nm pixels. (B) STORM image of actin filament shown in (A). From a 20,000 frame sequence with a 128 x 128 pixel frame size, a 10 msec exposure time and acquired at 52.5 frames per second. The STORM pixel size is 16 nm. All 20,000 frames were processed. The mean precision estimate is 17 nm. (C) As (B) but with only the first 5000 frames of the 20,000 frame sequence processed. The mean precision estimate is 18 nm.(D) As (B) but with only the last 5,000 frames of the 20,000 frame sequence processed. The mean precision estimate is 17 nm.(E) Graph of localizations per frame data from full 128 x 128 pixel frame view.

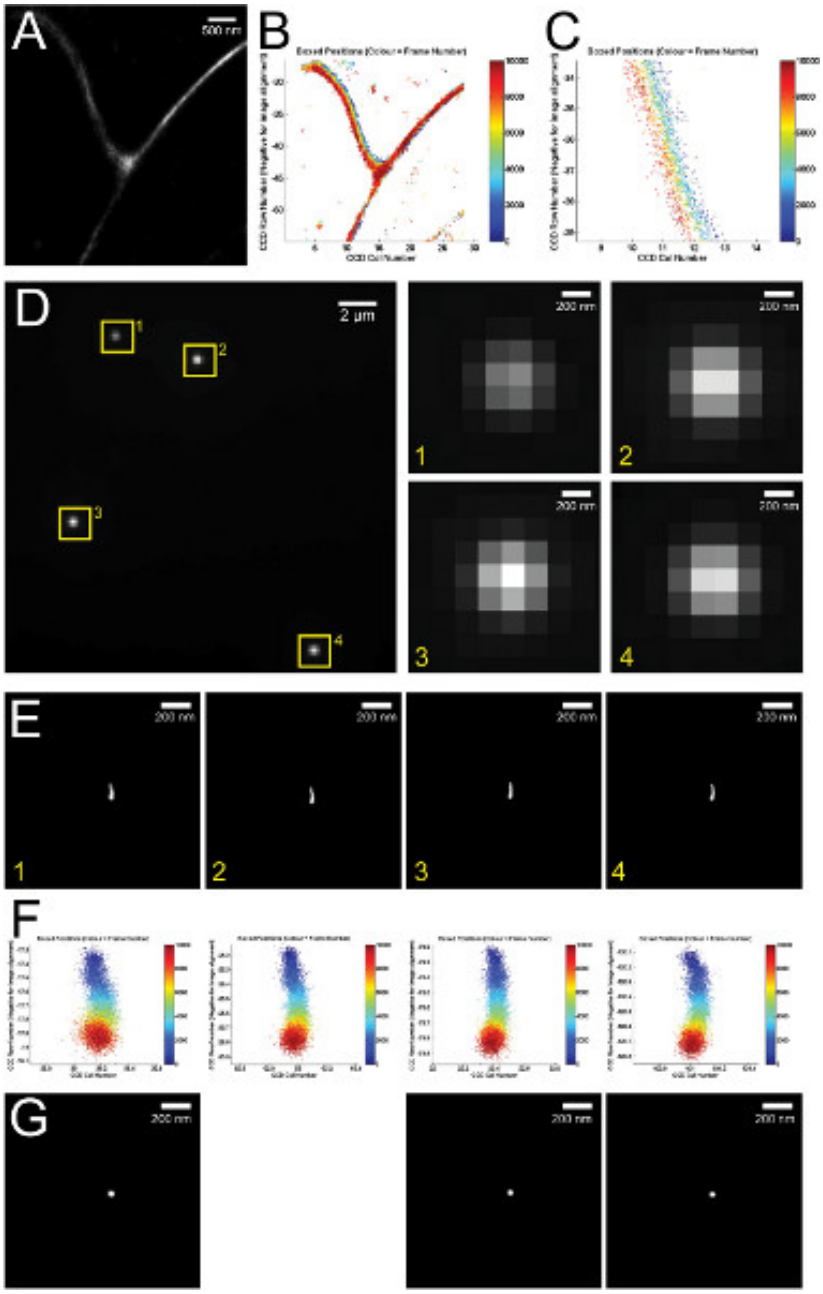

Figure 6. Lateral Drift. (A) STORM image of an actin filament reconstructed from a 10,000 frame sequence with a 64 x 64 pixel frame size, a 10 msec exposure time and taken at 64.6 frames per second. The STORM pixel size is 32 nm. The mean precision estimate is 32 nm. (B) A STORM image displayed using the 'Box Tracking' feature in rainSTORM. Localizations are displayed with a color corresponding to the frame number of when they were acquired, for example, localizations from early in the acquisition sequence are blue; localizations from late in the acquisition sequence are red. The displaced colors indicate that drift has occurred. (C) A zoomed in region of (A) displayed using the Box Tracking feature in rainSTORM. The displaced colors indicate drift has occurred. (D) A diffraction limited image of four 100 nm fluorescent beads, which can be used as fiducial markers. Pixel size 160 nm. Numbers 1-4 show cropped and zoomed beads individually. (E) Each fluorescent bead corresponding to (D) reconstructed in rainSTORM from a 10,000 frame sequence with a 128 x 128 pixel frame size, a 10 msec exposure time and acquired at 52.5 frames per second. The STORM pixel size is 5 nm. The mean precision estimate is 7 nm. (F) Beads corresponding to (D) and (E), displayed using the 'Box Tracking' feature. The displaced colors indicate drift has occurred. (G) Using bead number 2 as the reference, beads 1, 3 and 4 are displayed after the 'Subtract Drift' feature is used in rainSTORM. Comparison with (E) shows that the lateral drift has been corrected. The STORM pixel size is 5 nm. Click here to view larger figure.

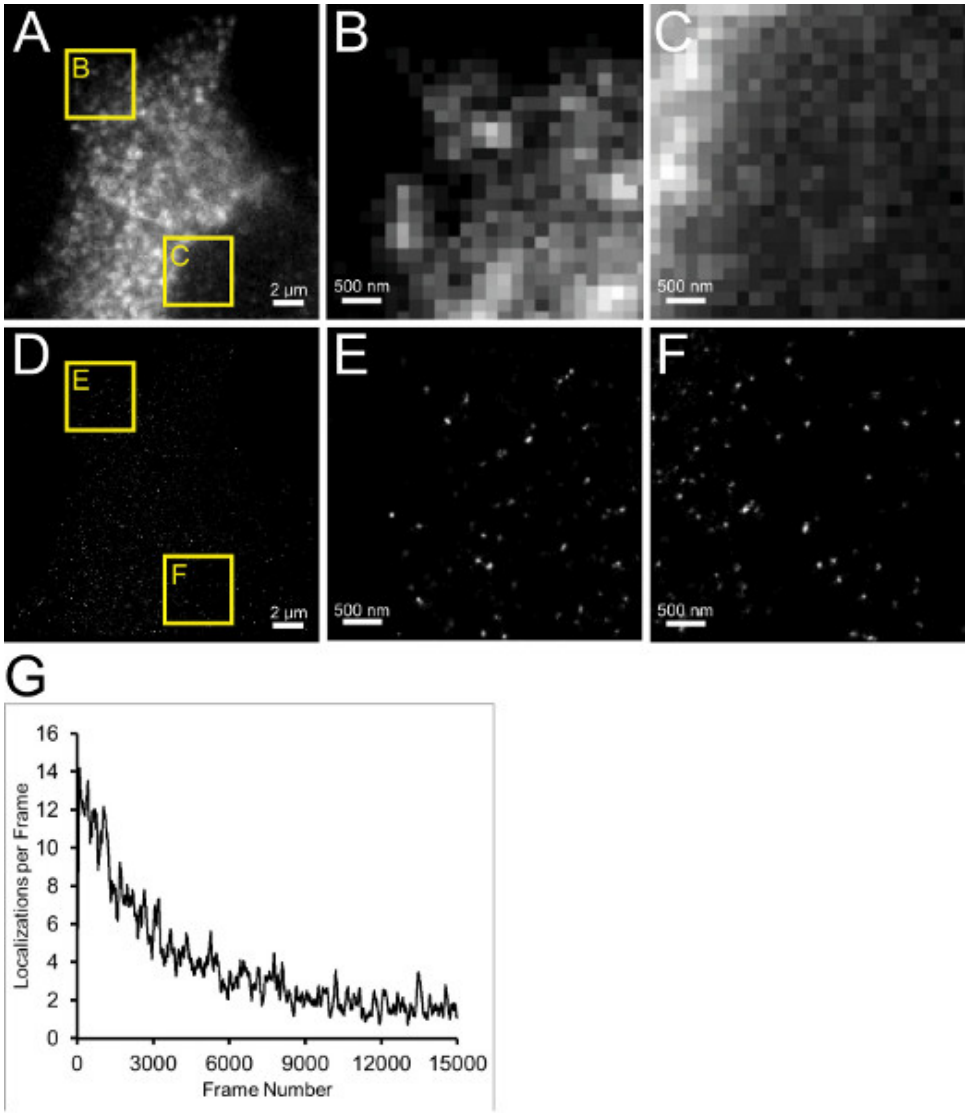

Figure 7. Typical EGF Data. (A) Diffraction limited image of part of a HeLa cell focused at the basal cell surface. Yellow boxes indicate zoomed in regions of interest shown in (B) & (C). (B) Zoomed in diffraction limited image from the region near the edge of the cell (box B). (C) Zoomed in diffraction limited image from region under the nucleus (box C). (D) STORM image corresponding to (A). From a 10,000 frame sequence with a 128 x 128 pixel frame size, a 10 msec exposure time and acquired at 52.5 frames per second. The STORM pixel size is 25 nm. The mean precision estimate is 21 nm. (E) STORM image corresponding to box E (D). (F) STORM image corresponding to box F (D). (G) Localizations per frame data from (D). Click here to view larger figure.

Videos 1-4. Videos correspond to **Figure 2A** with varying dextran concentrations: 1= high, 2= medium, 3= low, 4 =none). 10,000 frame sequences with 128 x 128 pixel frame sizes, acquired with a 10 msec exposure time at 52.5 frames per second. Click here to view video 1, video 2, video 3, video 4

Videos 5-6. Videos correspond to **Figure 3 A & B. Video 5** is pre-wash and **Video 6** is post-wash after unbound fluorophores have been removed. 15,000 frame sequences using a 128 x 128 pixel frame size, a 10 msec exposure time and acquired at 52.5 frames per second. Click here to view video 5, video 6.

Video 7. Video showing the raw frame sequence that was processed to generate the STORM image in **Figure 4E**. 10,000 frame sequence with a 128 x 128 pixel frame size, a 10 msec exposure time and acquired at 52.5 frames per second. Click here to view video 7.

Video 8. Video showing the raw frame sequence that was processed to generate the STORM image in **Figure 5B**. 20,000 frame sequence with a 128 x 128 pixel frame size, a 10 msec exposure time and acquired at 52.5 frames per second. Click here to view video 8.

Video 9. Video showing the raw frame sequence that was processed to generate the STORM image in **Figure 6A**. 10,000 frame sequence with a 64 x 64 pixel frame size, a 10 msec exposure time and taken at 64.6 frames per second. Click here to view video 9.

Video 10. Video showing the raw frame sequence that was processed to generate the STORM image in **Figure 7D**. 10,000 frame sequence with a 128 x 128 pixel frame size, a 10 msec exposure time and acquired at 52.5 frames per second. Click here to view video 10.

Discussion

We show with some simple test samples and the freely-available processing software rainSTORM it is possible to optimize STORM super-resolution imaging. These tools and methods will provide useful starting points for new users and ways for experienced users to increase confidence in their microscopes and their use of them to study biological and cellular structures with unprecedented detail. By using a combination of samples with known or well-understood structures and an algorithm that can produce a number of useful image quality metrics, such as mean precision estimates, localization number and histograms showing it is possible to improve image quality and to have greater confidence in the STORM imaging process. There is no one-size fits all approach to acquiring the data as there are a number of different commercial and self-built microscope configurations that can be used. Moreover, there are many sample preparation and image acquisition steps which can influence the final image therefore having software tools and test samples is critical to understanding and optimizing STORM image quality.

In addition these protocols can provide useful and less ambiguous ways of troubleshooting any problems that may arise. For example the dextran sample is a very useful way to identify if there is any laser beam misalignment or uneven illumination of the sample. If there are concerns that the switching buffer may not be working a very simple visual test to see if there is any 'blinking' will help. Actin filaments are a useful way of measuring resolution using FWHM comparisons as well as highlighting drift and mislocalization artifacts. However, it should be noted that as localization-based super-resolution methods can be fluorophore density sensitive, notwithstanding the other contributing factors, such as exposure times, frame rates, laser powers and the way the image is processed, it is impossible to assign a resolution to a particular microscope and assume that all images will have that resolution. What is possible, however, is to measure various aspects of resolution such as mean localization precisions, localization number and drift [27]. Even if fiducial markers cannot be incorporated into every experiment they can, at least, be used to characterize a microscope system, its environment and better understand operational considerations such as how much time is required to reach thermal equilibrium after start up. As well as correcting for lateral drift, fiducial markers can be used to characterize and correct for axial drift, although this requires the use of an astigmatic lens and a feedback mechanism to correct the sample position whilst the images are being acquired [43]. Commercial super-resolution systems will usually include some sort of stability control or focus-lock mechanism, which may be a more practical solution for correcting focus drift.

There are alternatives to non-specifically coating the glass with dextran, such as using dyes directly or other conjugate molecules, such as secondary antibodies. A limitation of these approaches is that the number of molecules bound to the glass is not known. Alternative filamentous structures that have been used include microtubules [28] and DNA[21]. However, the combination of very small size and convenient commercially available reagents make actin an attractive alternative, particularly as the separation distance of diverging or branched filaments can also be a useful measurement of system performance [27].

There is room for further development of test samples, despite recent progress in this area [28,29,46,47]. In particular, multi-color imaging presents a number of challenges in all 3 main aspects of the imaging, sample labeling, image acquisition (hardware), and software (image processing and alignment). There have a been a number of publications addressing these aspects [4-6] and it is therefore clear that appropriate test samples and methodologies are critical to generating and reliably interpreting these types of images. Indeed, recently it was shown that dSTORM could be used to take two color images of, and resolve, the highly symmetrical nature of the nuclear pore complex and the authors suggested that this would be an ideal way to assess performance of chromatic aberration corrections [45]. Another interesting approach is the use of DNA origami to create a nanoruler, which creates the possibility of positioning fluorophores at specific sub-diffraction distances apart [46]. This provides a way of assessing resolution and making distance measurements. However, the ultimate aim is to apply these super-resolution techniques to non-idealized samples, such as cells, which are complex three dimensional structures. In this case, a combination of more thorough understanding of the technique combined with software tools that aid the user in acquiring data, processing it in appropriate ways, and providing image metrics is likely to be the ultimate answer. [28,29,47,48]

Disclosures

We have nothing to disclose.

Acknowledgements

We acknowledge funding from the Chemical and Biological Metrology programme of the UK's National Measurement Office. We thank Sebastian van de Linde, Miklos Erdelyi and Eric Rees for technical advice and suggestions. We thank Miklos Erdelyi, Eric Rees and Max Ryadnov for helpful comments and discussions on this manuscript.

References

1. Galbraith, C. & Galbraith, J. Super-resolution microscopy at a glance. *Journal of Cell Science.* **124**, 1607-1611, doi:10.1242/jcs.080085 (2011).
2. Toomre, D. & Bewersdorf, J. A New Wave of Cellular Imaging. *Annual Review of Cell and Developmental Biology.* **26**, 285-314, doi: 10.1146/annurev-cellbio-100109-104048 (2010).
3. Bates, M., Huang, B., Dempsey, G., & Zhuang, X. Multicolor Super-Resolution Imaging with Photo-Switchable Fluorescent Probes. *Science.* **317**, 1749-1753, doi: 10.1126/science.1146598 (2007).
4. Bates, M., Dempsey, G., Chen, K.H., & Zhuang, X. Multicolor Super-Resolution Fluorescence Imaging via Multi-Parameter Fluorophore Detection. *Chemphyschem : a European journal of chemical physics and physical chemistry.* **13**, 99-107, doi:10.1002/cphc.201100735 (2012).

5. Testa, I., *et al.* Multicolor fluorescence nanoscopy in fixed and living cells by exciting conventional fluorophores with a single wavelength. *Biophysical journal.* **99**, 2686-2694, doi: 10.1016/j.bpj.2010.08.012 (2010).
6. Baddeley, D., *et al.* 4D Super-Resolution Microscopy with Conventional Fluorophores and Single Wavelength Excitation in Optically Thick Cells and Tissues. *PLoS ONE.* **6**, doi: 10.1371/journal.pone.0020645 (2011).
7. Shtengel, G., *et al.* Interferometric fluorescent super-resolution microscopy resolves 3D cellular ultrastructure. *Proceedings of the National Academy of Sciences of the United States of America.* **106**, 3125-3130, doi: 10.1073/pnas.0813131106 (2009).
8. Huang, B., Jones, S., Brandenburg, B., & Zhuang, X. Whole-cell 3D STORM reveals interactions between cellular structures with nanometer-scale resolution. *Nature Methods.* **5**, 1047-1052, doi: 10.1038/nmeth.1274 (2008).
9. Huang, B., Wang, W., Bates, M., & Zhuang, X. Three-Dimensional Super-Resolution Imaging by Stochastic Optical Reconstruction Microscopy. *Science*. **319**, 810-813, doi: 10.1126/science.1153529 (2008).
10. Juette, M., *et al.* Three-dimensional sub-100 nm resolution fluorescence microscopy of thick samples. *Nat Meth.* **5**, 527-529, doi: 10.1038/nmeth.1211 (2008).
11. Vaziri, A., Tang, J., Shroff, H., & Shank, C. Multilayer three-dimensional super resolution imaging of thick biological samples. *Proceedings of the National Academy of Sciences of the United States of America*. **105**, 20221-20226, doi: 10.1073/pnas.0810636105 (2008).
12. York, A., Ghitani, A., Vaziri, A., Davidson, M., & Shroff, H. Confined activation and subdiffractive localization enables whole-cell PALM with genetically expressed probes. *Nature Methods.* **8**, 327-333, doi: 10.1038/nmeth.1571 (2011).
13. Jones, S., Shim, S.-H., He, J., & Zhuang, X. Fast, three-dimensional super-resolution imaging of live cells. *Nature Methods.* **8**, 499-505, doi: 10.1038/nmeth.1605 (2011).
14. Shroff, H., Galbraith, C., Galbraith, J., & Betzig, E. Live-cell photoactivated localization microscopy of nanoscale adhesion dynamics. *Nature Methods.* **5**, 417-423, doi: 10.1038/nmeth.1202 (2008).
15. Hess, S., *et al.* Dynamic clustered distribution of hemagglutinin resolved at 40 nm in living cell membranes discriminates between raft theories. *Proceedings of the National Academy of Sciences.* **104**, 17370-17375, doi: 10.1073/pnas.0708066104 (2007).
16. Wombacher, R., *et al.* Live-cell super-resolution imaging with trimethoprim conjugates. *Nature Methods*. **7**, 717-719, doi: 10.1038/nmeth.1489 (2010).
17. Klein, T., *et al.* Live-cell dSTORM with SNAP-tag fusion proteins. *Nature Methods.* **8**, 7-9, doi: 10.1038/nmeth0111-7b (2011).
18. Folling, J., *et al.* Fluorescence nanoscopy by ground-state depletion and single-molecule return. *Nature Methods.* **5**, 943-945, doi: 10.1038/nmeth.1257 (2008).
19. Betzig, E., *et al.* Imaging Intracellular Fluorescent Proteins at Nanometer Resolution. *Science*. **313**, 1642-1645, doi: 10.1126/science.1127344 (2006).
20. Hess, S.T., Girirajan, T.P., & Mason, M.D. Ultra-high resolution imaging by fluorescence photoactivation localization microscopy. *Biophys J.* **91**, 4258-4272, doi:10.1529/biophysj.106.091116 (2006).
21. Rust, M., Bates, M., & Zhuang, X. Sub-diffraction-limit imaging by stochastic optical reconstruction microscopy (STORM). *Nature Methods*. **3**, 793-796, doi: 10.1038/nmeth929 (2006).
22. Hofmann, M., Eggeling, C., Jakobs, S., & Hell, S.W. Breaking the diffraction barrier in fluorescence microscopy at low light intensities by using reversibly photoswitchable proteins. *Proc. Natl. Acad. Sci. U.S.A.* **102**, 17565-17569, doi:10.1073/pnas.0506010102 (2005).
23. Thompson, R.E., Larson, D.R., & Webb, W.W. Precise nanometer localization analysis for individual fluorescent probes. *Biophys J.* **82**, 2775-2783, doi:10.1016/S0006-3495(02)75618-X (2002).
24. Wolter, S., *et al.* Real-time computation of subdiffraction-resolution fluorescence images. *Journal of Microscopy.* **237**, 12-22, doi: 10.1111/j.1365-2818.2009.03287.x (2010).
25. Wolter, S., *et al.* rapidSTORM: accurate, fast open-source software for localization microscopy. *Nat. Methods.* **9**, 1040-1041, doi:10.1038/nmeth.2224 (2012).
26. Henriques, R., *et al.* QuickPALM: 3D real-time photoactivation nanoscopy image processing in ImageJ. *Nature Methods.* **7**, 339-340, doi: 10.1038/nmeth0510-339 (2010).
27. Rees, E., *et al.* Blind Assessment of Localisation Microscope Image Resolution. *Journal of Optical Nanoscopy.* **1**, 12, doi:10.1186/2192-2853-1-12 (2012).
28. Dempsey, G., Vaughan, J., Chen, K., Bates, M., & Zhuang, X. Evaluation of fluorophores for optimal performance in localization-based super-resolution imaging. *Nat Meth.* **8**, 1027-1036, doi: 10.1038/nmeth.1768 (2011).
29. van de Linde, S., *et al.* Direct stochastic optical reconstruction microscopy with standard fluorescent probes. *Nature protocols*. **6**, 991-1009, doi: 10.1038/nprot.2011.336 (2011).
30. Heilemann, M., *et al.* Subdiffraction-Resolution Fluorescence Imaging with Conventional Fluorescent Probes. *Angewandte Chemie International Edition.* **47**, 6172-6176, doi: 10.1002/anie.200802376 (2008).
31. Owen, D.M., Sauer, M., & Gaus, K. Fluorescence localization microscopy: The transition from concept to biological research tool. *Commun Integr Biol.* **5**, 345-349, doi:10.4161/cib.20348 (2012).
32. van de Linde, S., Wolter, S., Heilemann, M., & Sauer, M. The effect of photoswitching kinetics and labeling densities on super-resolution fluorescence imaging. *Journal of biotechnology.* **149**, 260-266, doi: 10.1016/j.jbiotec.2010.02.010 (2010).
33. Veatch, S., *et al.* Correlation Functions Quantify Super-Resolution Images and Estimate Apparent Clustering Due to Over-Counting. *PLoS ONE.* **7**, e31457, doi: 10.1371/journal.pone.0031457 (2012).
34. Holden, S., Uphoff, S., & Kapanidis, A. DAOSTORM: an algorithm for high- density super-resolution microscopy. *Nature methods.* **8**, 279-280, doi: 10.1038/nmeth0411-279 (2011).
35. Cox, S., *et al.* Bayesian localization microscopy reveals nanoscale podosome dynamics. *Nat Methods*. **9**, 195-200, doi:10.1038/nmeth.1812 (2012).
36. Mukamel, E., Babcock, H., & Zhuang, X. Statistical deconvolution for superresolution fluorescence microscopy. *Biophysical Journal*. **102**, 2391-2400, doi: 10.1016/j.bpj.2012.03.070 (2012).
37. Shim, S.H., *et al.* Super-resolution fluorescence imaging of organelles in live cells with photoswitchable membrane probes. *Proc. Natl. Acad. Sci. U. S. A.* **109**, 13978-13983, doi:10.1073/pnas.1201882109 (2012).
38. Parkar, N.S., *et al.* Vesicle formation and endocytosis: function, machinery, mechanisms, and modeling. *Antioxid Redox Signal.* **11**, 1301-1312, doi:10.1089/ARS.2008.2397 (2009).
39. Clague, M.J. & Urbe, S. The interface of receptor trafficking and signalling. *J Cell Sci.* **114**, 3075-3081 (2001).
40. van de Linde, S., Sauer, M., & Heilemann, M. Subdiffraction-resolution fluorescence imaging of proteins in the mitochondrial inner membrane with photoswitchable fluorophores. *Journal of Structural Biology.* **164**, 250-254, doi: 10.1016/j.jsb.2008.08.002 (2008).

41. Heilemann, M., Margeat, E., Kasper, R., Sauer, M., & Tinnefeld, P. Carbocyanine Dyes as Efficient Reversible Single-Molecule Optical Switch. *Journal of the American Chemical Society.* **127**, 3801-3806, doi: 10.1021/ja044686x (2005).
42. Heilemann, M., van de Linde, S., Mukherjee, A., & Sauer, M. Super-Resolution Imaging with Small Organic Fluorophores. *Angewandte Chemie International Edition.* **48**, 6903-6908, doi: 10.1002/anie.200902073 (2009).
43. Lee, S.H., *et al.* Using fixed fiduciary markers for stage drift correction. *Opt Express.* **20**, 12177-12183, doi:10.1364/OE.20.012177 (2012).
44. Mlodzianoski, M., *et al.* Sample drift correction in 3D fluorescence photoactivation localization microscopy. *Optics express.* **19**, 15009-15019 (2011).
45. Löschberger, A., *et al.* Super-resolution imaging visualizes the eightfold symmetry of gp210 proteins around the nuclear pore complex and resolves the central channel with nanometer resolution. *Journal of Cell Science.* **125**, 570-575, doi: 10.1242/jcs.098822 (2012).
46. Steinhauer, C., Jungmann, R., Sobey, T.L., Simmel, F.C., & Tinnefeld, P. DNA origami as a nanoscopic ruler for super-resolution microscopy. *Angew Chem Int Ed Engl.* **48**, 8870-8873, doi:10.1002/anie.200903308 (2009).
47. Laevsky, G.S. & O'Connell, C.B. Comparative and practical aspects of localization-based super-resolution imaging. *Current protocols in cytometry / editorial board, J. Paul Robinson, managing editor ... [et al.]* Chapter 2, Unit2 20, doi:10.1002/0471142956.cy0220s63 (2013).
48. Gould, T., Verkhusha, V., & Hess, S. Imaging biological structures with fluorescence photoactivation localization microscopy. *Nature protocols.* **4**, 291-308, doi:citeulike-article-id:4349535doi: 10.1038/nprot.2008.246 (2009).